

Driven-Dissipative Supersolid in a Ring Cavity

Farokh Mivehvar,^{1,*} Stefan Ostermann,¹ Francesco Piazza,² and Helmut Ritsch^{1,†}

¹*Institut für Theoretische Physik, Universität Innsbruck, A-6020 Innsbruck, Austria*

²*Max-Planck-Institut für Physik komplexer Systeme, D-01187 Dresden, Germany*

Supersolids are characterized by the counter-intuitive coexistence of superfluid and crystalline order. Here we study a supersolid phase emerging in the steady state of a driven-dissipative system. We consider a transversely pumped Bose-Einstein condensate trapped along the axis of a ring cavity and coherently coupled to a pair of degenerate counter-propagating cavity modes. Above a threshold pump strength the interference of photons scattered into the two cavity modes results in an emergent superradiant lattice, which spontaneously breaks the continuous translational symmetry towards a periodic atomic pattern. The crystalline steady state inherits the superfluidity of the Bose-Einstein condensate, thus exhibiting genuine properties of a supersolid. A gapless collective Goldstone mode correspondingly appears in the superradiant phase, which can be non-destructively monitored via the relative phase of the two cavity modes on the cavity output. Despite cavity-photon losses the Goldstone mode remains undamped, indicating the robustness of the supersolid phase.

Introduction.—A supersolid behaves as both a crystalline solid and a superfluid. It *spontaneously* breaks two continuous symmetries, namely the external spatial translation invariance and the internal superfluid gauge invariance. That is, it simultaneously possesses diagonal (i.e., density) and off-diagonal (i.e., superfluid) long-range orders [1]. This paradoxical state of matter has been predicted almost 50 years ago to exist in solid helium-4 [2–6]. Despite intensive experimental efforts [7, 8], supersolidity has not been conclusively observed in solid helium-4 yet [9–11].

In a different direction, very recently clear signatures of supersolidity have been observed in weakly interacting ultracold atomic systems. At MIT, synthetic spin-orbit coupling was induced in a multi-component Bose-Einstein condensate (BEC) [12]. The ground state of the system spontaneously breaks the continuous translational symmetry and forms a density modulated stripe pattern, while maintaining superfluidity of the BEC. At ETH, a transversally driven BEC was symmetrically coupled to two modes of two crossed linear cavities [13]. Interference of pump-laser photons and photons scattered into the cavity modes yields an emergent superradiant optical lattice for the BEC, which spontaneously breaks the continuous translational invariance towards a density-modulated superfluid state. In another experiment at MIT [14], a BEC illuminated by two non-interfering counter-propagating lasers exhibited collective Rayleigh scattering, resulting in spontaneous crystallization of both matter and light [15, 16]. However, the potential appearance of supersolidity in this system has not been thoroughly investigated yet.

Based on the state of the art in experimental quantum-gas cavity QED [17–22], we propose a novel scheme to experimentally realize and study supersolidity in a BEC trapped within a ring resonator [23–27]. The BEC, which is transversely illuminated by a standing-wave laser, is trapped along the cavity axis in a quasi one-dimensional geometry and dispersively coupled to a

pair of degenerate counter-propagating field modes as depicted in Fig. 1. This comprises an intrinsically driven-dissipative system due to the pump laser and cavity-photon losses [28]. Therefore, the emergent supersolid above the self-ordering threshold is the steady-state of the system. The interesting questions which arise are if and how the supersolid features are modified with respect to thermal equilibrium.

Above a critical laser intensity, the collective constructive scattering of pump-laser photons into the cavity modes results in an emergent superradiant optical lattice. In contrast to the standing-wave linear cavity [29], the running-wave ring cavity respects the *continuous* spatial translational symmetry. Hence, the location of the emerging optical lattice is not pre-determined by the cavity mirrors and *spontaneously* breaks the continuous translational symmetry, similar to the emergent optical

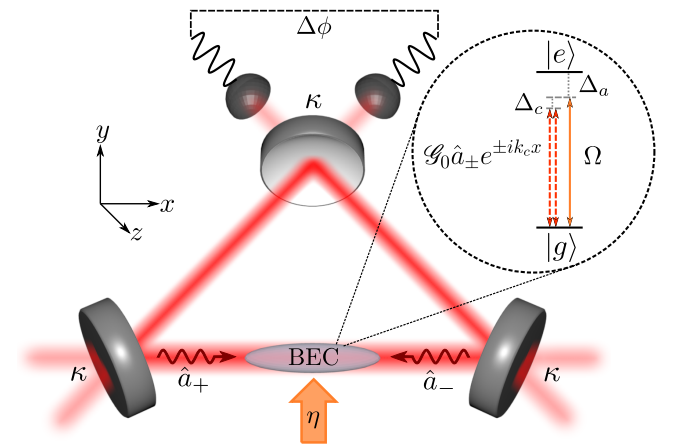


FIG. 1. Schematic sketch of a BEC inside a ring cavity. An internal atomic transition $|g\rangle \leftrightarrow |e\rangle$ is off-resonantly driven by a transverse plane-wave laser with Rabi frequency Ω . This transition is also off-resonantly coupled to a pair of degenerate, counter-propagating cavity modes \hat{a}_{\pm} with coupling strength $\mathcal{G}(x) = \mathcal{G}_0 e^{\pm ik_c x}$.

lattice in the crossed-cavity experiment [13]. Nevertheless, in the latter the continuous symmetry is merely an approximate and fine-tuned symmetry [30–32]. A similar continuous symmetry breaking can also occur for atoms trapped close to optical fibers [33, 34].

The emergent superradiant lattice drives the BEC into a density modulated state — i.e., a crystalline phase — with the spontaneously broken continuous translational symmetry [see Fig. 2(b)]. It, nevertheless, inherits superfluidity of the BEC with a long-range phase coherence. Therefore, the resultant steady state in the superradiant phase is a supersolid. As the cavity comprises an open system, the continuous symmetry breaking can be monitored non-destructively in real time via the cavity output, namely via the *relative phase* of the two cavity modes [17, 18]. In particular, the relative phase takes a random value between 0 and 2π in the superradiant phase, spontaneously breaking the continuous $U(1)$ symmetry [see the inset of Fig. 2(b)]. In fact, at the onset of superradiance a superposition of field amplitudes with different phases correlated with density fluctuations emerges, forming a highly entangled atom-field state. This state subsequently collapses to a state with a certain random relative phase via quantum jumps induced by cavity photon losses [35–37].

Analysis of collective excitations confirms the supersolidity of the superradiant steady state. At the onset of the superradiant phase transition, where the continuous $U(1)$ symmetry is spontaneously broken, a gapless Goldstone mode appears in the spectrum of collective excitations. Unlike all other collective modes, the Goldstone mode remains undamped despite cavity losses (see Fig. 3). This is due to the fact that photon losses do not affect the relative phase and preserve the $U(1)$ symmetry. This is in contrast to the supersolid realized in the crossed-cavity setup, where the origin of the $U(1)$ symmetry is different and associated with the freedom of the photon redistribution between the two cavity modes [13]. Therefore, photon losses do not respect the $U(1)$ symmetry and should result in damping of the Goldstone mode [38].

Model.—Consider bosonic two-level atoms trapped along the axis of a ring resonator by a tight confining potential along the transverse directions. The atoms are illuminated from the side by an off-resonant, standing-wave external pump laser as depicted in Fig. 1, which induces the transition $|g\rangle \leftrightarrow |e\rangle$ with the Rabi frequency Ω . Furthermore, the transition $|g\rangle \leftrightarrow |e\rangle$ is also off-resonantly coupled to a pair of degenerate, counter-propagating cavity modes \hat{a}_\pm , with coupling strength $\mathcal{G}(x) = \mathcal{G}_0 e^{\pm ik_c x}$. The cavity modes are initially in the vacuum state. The pump and cavity frequencies, respectively, ω_p and $\omega_c = ck_c$ are assumed to be near resonant with each other, but far-red detuned with respect to the atomic frequency ω_a .

In the dispersive regime $|\Delta_a| \equiv |\omega_p - \omega_a| \gg \{\Omega, \mathcal{G}_0\}$, the atomic excited state $|e\rangle$ reaches quickly to a steady

state with a negligible population and its dynamics can be adiabatically eliminated [28]. This yields an effective Hamiltonian for the atomic ground state and the cavity modes, $H_{\text{eff}} = \int \hat{\psi}^\dagger(x) \mathcal{H}_{\text{eff}}^{(1)} \hat{\psi}(x) dx - \hbar \Delta_c (\hat{a}_+^\dagger \hat{a}_+ + \hat{a}_-^\dagger \hat{a}_-)$, with the effective single-particle atomic Hamiltonian density:

$$\begin{aligned} \mathcal{H}_{\text{eff}}^{(1)} = & -\frac{\hbar^2}{2m} \frac{\partial^2}{\partial x^2} + \hbar U \left(\hat{a}_+^\dagger \hat{a}_+ + \hat{a}_-^\dagger \hat{a}_- + \hat{a}_+^\dagger \hat{a}_- e^{-2ik_c x} \right. \\ & \left. + \hat{a}_-^\dagger \hat{a}_+ e^{2ik_c x} \right) + \hbar \eta \left(\hat{a}_+ e^{ik_c x} + \hat{a}_- e^{-ik_c x} + \text{H.c.} \right). \end{aligned} \quad (1)$$

Here, $\hat{\psi}(x)$ is the bosonic annihilation field operator for the atomic ground state. We have introduced the cavity detuning with respect to the pump $\Delta_c \equiv \omega_p - \omega_c$, the maximum depth of the optical potential per photon due to two-photon scattering between cavity modes $\hbar U \equiv \hbar \mathcal{G}_0^2 / \Delta_a$ and the maximum depth of the optical potential per photon due to the two-photon scattering between pump and cavity modes (or the effective cavity-pump strength) $\hbar \eta \equiv \hbar \mathcal{G}_0 \Omega / \Delta_a$. Although finite atom-atom interactions are needed to ensure the superfluidity of the BEC, we have assumed them to be negligibly small with respect to the cavity-mediated interactions. This is quantitatively a good approximation for typical cavity-QED experiments, including the recent observation of the supersolid [13]. Finally, the cavity-photon losses with rate κ are included via Lindblad operators in the master equation for the density matrix ρ : $\mathcal{L}\rho = \kappa \sum_{\ell=+,-} \left(2\hat{a}_\ell \rho \hat{a}_\ell^\dagger - \left\{ \hat{a}_\ell^\dagger \hat{a}_\ell, \rho \right\} \right)$.

The system possesses a continuous $U(1)$ symmetry, as the effective Hamiltonian H_{eff} and the Lindblad operators are invariant under the simultaneous spatial translation $x \rightarrow \mathcal{T}_X x = x + X$ and cavity-phase rotations $\hat{a}_\pm \rightarrow \mathcal{U}_X \hat{a}_\pm = \hat{a}_\pm e^{\mp ik_c X}$. This $U(1)$ symmetry is spontaneously broken in the superradiant phase, as illustrated in the inset of Fig. 2(b), where $\langle \hat{a}_\pm \rangle$ acquire non-zero values with arbitrary phases.

Mean-Field Approach and Continuous Symmetry Breaking.—In the thermodynamic limit, where the mean-field approximation becomes accurate [39], the system is described by a set of three coupled mean-field (Heisenberg) equations for the cavity-field amplitudes $\langle \hat{a}_\pm(t) \rangle = \alpha_\pm(t) = |\alpha_\pm(t)| e^{i\phi_\pm(t)}$ and the atomic condensate wavefunction $\langle \hat{\psi}(x, t) \rangle = \psi(x, t) = \sqrt{n(x, t)} e^{i\theta(t)}$ [40],

$$\begin{aligned} i \frac{\partial}{\partial t} \alpha_\pm &= (-\Delta_c + UN - i\kappa) \alpha_\pm + UN_{\pm 2} \alpha_\mp + \eta \mathcal{N}_{\pm 1}, \\ i \hbar \frac{\partial}{\partial t} \psi &= \mathcal{H}_{\text{eff}}^{(1)} \psi, \end{aligned} \quad (2)$$

where $N = \int n(x) dx$ is the number of the particles. One can identify $\mathcal{N}_{\pm 1} \equiv \int n(x) e^{\mp ik_c x} dx$ as the atomic order parameters, dual to the cavity order parameters α_\pm , which characterize the probability of the photon scattering between the pump and cavity modes with $\mp \hbar k_c$

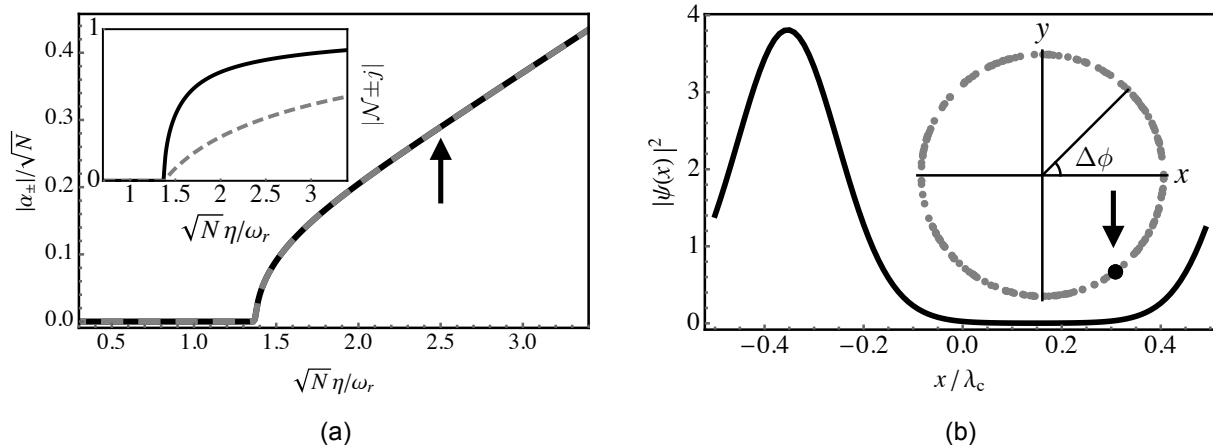


FIG. 2. Dicke superradiant phase transition and atomic self-organization. (a) The absolute values of the rescaled cavity-field amplitudes $|\alpha_{\pm}|/\sqrt{N}$ (black solid and grey dashed curves, respectively) are shown as a function of the rescaled effective cavity-pump strength $\sqrt{N}\eta/\omega_r$. The superradiant phase transition occurs at the critical pump strength $\sqrt{N}\eta_c \approx 1.38\omega_r$, where $|\alpha_+| = |\alpha_-| > 0$. The inset shows the absolute values of the quantities $|N_{\pm 1}|$ (the solid black curve) and $|N_{\pm 2}|$ (the dashed gray curve) as a function of $\sqrt{N}\eta/\omega_r$. (b) A typical self-ordered atomic density profile is shown for $\sqrt{N}\eta = 2.5\omega_r$ with $\Delta\phi \approx 1.71\pi$ and $\Phi \approx 0.09\pi$, where $\Delta\phi$ fixes the position of the density maximum $x_m \approx -0.35\lambda_c$. The inset illustrates the distribution of $\Delta\phi$ for 200 numerical runs for $\sqrt{N}\eta = 2.5\omega_r$, exhibiting the continuous $U(1)$ symmetry breaking. The parameters are set to $(\Delta_c, U, \kappa) = (-8, -1, 2)\omega_r$.

momentum transfer to the atoms along the cavity axis x . Whereas, $N_{\pm 2} \equiv \int n(x)e^{\mp 2ik_c x} dx$ quantifies the probability of the photon redistribution between the two cavity modes with $\mp 2\hbar k_c$ momentum transfer to the atoms in the x direction.

We self-consistently find the steady-state solutions of Eq. (2) by setting $\partial_t \alpha_{\pm} = 0$ and $i\hbar \partial_t \psi = \mu \psi$, with μ being the chemical potential. Figure 2(a) shows the absolute values of the rescaled cavity-mode amplitudes $|\alpha_{\pm}|/\sqrt{N}$ (black solid and grey dashed curves, respectively) as a function of the rescaled effective pump strength $\sqrt{N}\eta/\omega_r$, with $\omega_r \equiv \hbar k_c^2/2m$ being the recoil frequency. Below the threshold pump strength $\sqrt{N}\eta_c \approx 1.38\omega_r$, the cavity modes are empty and the BEC is uniform. By increasing the pump strength above η_c the system undergoes a superradiant phase transition, where the cavity amplitudes acquire non-zero values $|\alpha_+| = |\alpha_-| = |\alpha|$.

In the superradiant state, the relative phase $\Delta\phi \equiv (\phi_+ - \phi_-)/2$ of the two cavity modes is fixed in an arbitrary value between 0 and 2π and the continuous $U(1)$ symmetry is, therefore, spontaneously broken. This is illustrated in the inset of Fig. 2(b), where the distribution of $\Delta\phi$ is shown for 200 numerical runs for a pump strength $\sqrt{N}\eta = 2.5\omega_r$ [indicated by the arrow in Fig. 2(a)]. The emergent superradiant lattice has the form $V_{\text{SR}}(x) = 2U|\alpha|^2 \cos(2k_c x + 2\Delta\phi) + 4\eta|\alpha| \cos(k_c x + \Delta\phi) \cos(\Phi)$, with $\Phi \equiv (\phi_+ + \phi_-)/2$ being the total phase. The spontaneously chosen value of $\Delta\phi$ fixes the position of the lattice minima and thus of the BEC density modulation, spontaneously breaking the continuous transla-

tional invariance and resulting in a supersolid state. A typical self-ordered, λ_c -periodic atomic density profile is shown in Fig. 2(b) for $\sqrt{N}\eta = 2.5\omega_r$ with $\Delta\phi \approx 1.71\pi$ [the pronounced black dot indicated by the arrow in the inset of Fig. 2(b)] and $\Phi \approx 0.09\pi$.

The total phase Φ solely modifies the lattice amplitude, except the special case of $\Phi = \pi/2$ where the lattice spacing is reduced from λ_c to $\lambda_c/2$. Note that Φ is not random as it is invariant under the $U(1)$ phase rotation $\alpha_{\pm} \rightarrow \alpha_{\pm} e^{\mp ik_c X}$. The total phase Φ solely depends on κ , while the relative phase $\Delta\phi$ is independent of κ . This is because photon losses induce equal extra phase shifts for both cavity-field amplitudes. Therefore, the spontaneous $U(1)$ -symmetry breaking and thus the supersolid order persist even in the presence of dissipation.

Collective Excitations and the Goldstone Mode.—Let us now turn our attention to elementary excitations of the system, which include quantum fluctuations of both condensate wavefunction $\delta\psi(x, t) = \delta\psi^{(+)}(x)e^{-i\omega t} + [\delta\psi^{(-)}(x)]^* e^{i\omega^* t}$ and cavity-field amplitudes $\delta\alpha_{\pm}(t) = \delta\alpha_{\pm}^{(+)} e^{-i\omega t} + [\delta\alpha_{\pm}^{(-)}]^* e^{i\omega^* t}$ above the mean-field solutions $\psi_0(x)$ and $\alpha_{0\pm}$ (with the corresponding chemical potential μ_0). Linearizing Eq. (2) yields Bogoliubov-type equations for the quantum fluctuations [24, 41, 42],

$$\begin{aligned}
 i\frac{\partial}{\partial t}\delta\alpha_{\pm} &= (-\Delta_c + UN - i\kappa)\delta\alpha_{\pm} + UN_{\pm 2}^{(0)}\delta\alpha_{\mp} \\
 &\quad + \int A_{\pm}(\psi_0^*\delta\psi + \psi_0\delta\psi^*)dx, \\
 i\frac{\partial}{\partial t}\delta\psi &= \frac{1}{\hbar}\left(\mathcal{H}_{\text{eff}}^{(1)} - \mu_0\right)\delta\psi \\
 &\quad + \psi_0(A_+^*\delta\alpha_+ + A_-^*\delta\alpha_- + \text{H.c.}), \quad (3)
 \end{aligned}$$

where $\mathcal{N}_{\pm 2}^{(0)} = \int n_0(x) e^{\mp 2ik_c x} dx$ and we have defined $A_{\pm}(x) \equiv U(\alpha_{0\pm} + \alpha_{0\mp} e^{\mp 2ik_c x}) + \eta e^{\mp ik_c x}$ for shorthands. The Bogoliubov equations (3) can be recast in a matrix form,

$$\omega \mathbf{f} = \mathbf{M}_B \mathbf{f}, \quad (4)$$

where $\mathbf{f} = (\delta\alpha_+^{(+)}, \delta\alpha_+^{(-)}, \delta\alpha_-^{(+)}, \delta\alpha_-^{(-)}, \delta\psi^{(+)}, \delta\psi^{(-)})^T$ and \mathbf{M}_B is a non-Hermitian matrix; see the Supplemental Material for the details [40]. The eigenvalues ω of the Bogoliubov equations (4) yield collective excitation spectrum of the system. We numerically solve Eq. (4) in one unit cell (of length λ_c) with periodic boundary conditions to obtain the collective excitations ω .

Figure 3 shows the real part of the six lowest-lying excitation frequencies as a function of the effective cavity-pump strength $\sqrt{N}\eta/\omega_r$. At small pump strengths, the excitation spectra are weakly dependent on η and each branch is doubly degenerate. The lowest four collective excitations at frequencies $\sim \omega_r$ (solid blue and dashed red curves) and $\sim 4\omega_r$ (dotted orange and dashed-dotted brown curves) correspond to mainly atomic fluctuations with momenta $\pm\hbar k_c$ and $\pm 2\hbar k_c$, respectively. The highest two modes (dashed-dashed-dotted black and dotted-dotted-dashed gray curves) at frequencies $\sim -\Delta_c + UN = 7\omega_r$ are mostly photon-like fluctuations.

By increasing η the collective modes are increasingly mixed with each other and begin to split up. In particular, the lowest excitation softens and the excitation gap closes at the pump strength $\sqrt{N}\eta_G \approx 1.37\omega_r$. By increasing pump strength beyond η_G , the lowest excitation splits into two branches. The lower one (solid blue curve) remains pinned at zero energy, signaling that it is a *gapless* Goldstone mode corresponding to the spontaneously broken continuous $U(1)$ symmetry. The gapped branch instead corresponds to a Higgs amplitude mode. These are reminiscent of the recently observed Goldstone and Higgs modes in the crossed-cavity experiment [38]. The Goldstone mode in the crossed-cavity experiment, however, should have a small gap of a few ω_r due to the fact that the continuous $U(1)$ symmetry is an approximate symmetry [30]. Note that these are in sharp contrast to the self-organization in a linear cavity, where only a discrete \mathbf{Z}_2 symmetry is spontaneously broken and the first excitation gap closes at the critical pump strength but then re-opens again [24, 41, 43].

Due to a nonzero cavity-field decay rate $\kappa \neq 0$ the excitation frequencies can acquire imaginary parts, which would indicate the damping of the excitations [24, 41]. This would in turn result in friction forces on the atoms. Above the critical pump strength η_c , all the collective excitations except the gapless Goldstone mode acquire imaginary parts. This is illustrated in the inset of Fig. 3, which shows the imaginary part of the lowest mode as a function of $\sqrt{N}\eta/\omega_r$. Although it is damped for small pump strengths, it vanishes at the critical pump strength

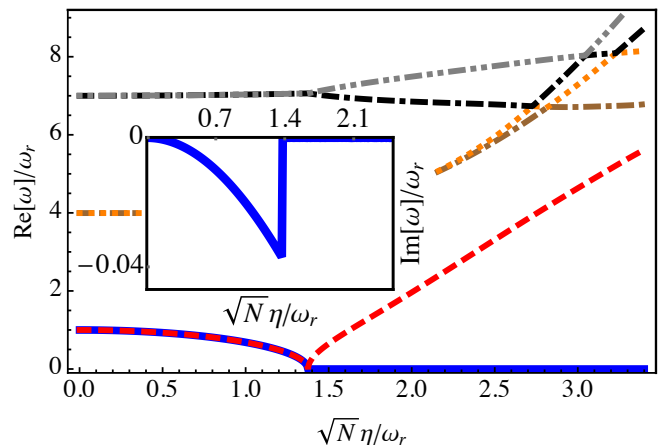


FIG. 3. (Color online) Low-lying collective excitations. The real part of the six lowest-lying excitation spectra are shown as a function of the rescaled effective cavity-pump strength $\sqrt{N}\eta/\omega_r$. By increasing $\sqrt{N}\eta/\omega_r$ from zero the lowest excitation, corresponding mainly to the atomic condensate fluctuations with momenta $\pm\hbar k_c$, softens and the excitation gap closes at $\sqrt{N}\eta_G \approx 1.37\omega_r$. By further increasing $\sqrt{N}\eta/\omega_r$, a gap does not open in the first excitation branch (the solid blue curve), indicating that this is a gapless Goldstone mode corresponding to the spontaneously broken continuous $U(1)$ symmetry. The inset shows the imaginary part of the Goldstone mode. The parameters are the same as Fig. 2.

$\sqrt{N}\eta_c \approx 1.38\omega_r$ (recall that the corresponding real part vanishes at the slightly lower pump strength η_G , where the damping reaches its maximum value), in agreement with the mean-field results [see Fig. 2(a)]. This means that the center of mass of the entire modulated BEC can move freely along the cavity axis without experiencing any friction, once again illustrating the supersolidity of the system. The fact that supersolidity survives even in presence of dissipation is due to the fact that the corresponding Lindblad operators respect the $U(1)$ -symmetry of the system. This is in contrast to the supersolid realized in the crossed-cavity setup, where the Goldstone mode involves photon-number redistribution between the two cavities and should therefore be damped by photon losses.

Around the critical point η_c , the atomic momentum states $\pm\hbar k_c$ are the dominant atomic fluctuations coupled to the cavity fluctuations. This can be seen from the inset of Fig. 2(a), where the quantities $|\mathcal{N}_{\pm j}|$ with $j = 1, 2$ are shown as a function of $\sqrt{N}\eta/\omega_r$. For $\eta \gtrsim \eta_c$, $\mathcal{N}_{\pm 1}$ (the black solid curve) are the dominant quantities. It is, therefore, a good approximation to restrict atomic fluctuations to the momentum states $\pm\hbar k_c$. Using the homogeneous solution (i.e., the solution below the Dicke transition) $\alpha_{0\pm} = 0$ and $\psi_0 = \sqrt{N}/\lambda_c$, one can diagonalize Eq. (4) in this restricted subspace. The zero frequency

$\omega = 0$ solution yields the critical pump strength [40],

$$\sqrt{N}\eta_c = \sqrt{\frac{(-\Delta_c + UN)^2 + \kappa^2}{4(-\Delta_c + UN)}} \sqrt{\omega_r} \approx 1.38\omega_r, \quad (5)$$

which is in full agreement with the numerical results.

Experimental Detection of the Supersolid State.—As discussed earlier, in our system the spontaneous breaking of the continuous translational symmetry corresponds to fixing the value of the relative phase of the two cavity modes. This can be monitored non-destructively by recombining the cavity outputs through a beam splitter. In particular, the system can be in real time repeatedly driven across the superradiant phase transition by sweeping the pump strength across the threshold to verify the uniform distribution of the relative phase in the interval $0 - 2\pi$, similar to experiments with linear cavities [13, 43]. Experimental setups coupling a BEC into fields of a ring cavity already exist for almost a decade now [19–22]. Therefore, the discussed phenomena could be observed with only minimal changes to current state-of-the-art experiments.

Outlook.—Our driven-dissipative supersolid is essentially different than other proposed driven-dissipative supersolid states in Jaynes-Cummings-Hubbard lattices [44, 45], in that the latter ones are only the lattice supersolid with a broken discrete symmetry and no gapless Goldstone mode [46]. Crucially due to the genuine supersolidity and existence of the undamped gapless Goldstone mode, our proposal may have applications in precision measurements. By monitoring the relative phase between the cavity modes one can non-destructively follow the displacement of the BEC in real time. However, there is no back-action of the light field onto the BEC motion (apart from the one induced by the measurement of the phase) due to the existence of the undamped gapless Goldstone mode. Therefore, it could be used as a free-falling zero temperature mass for gravitational acceleration measurements, as an alternative to the atomic fountains [47–50]. We defer the investigation of the performance of such a device to a future work.

FM is grateful to Tobias Donner and Manuele Landini for fruitful discussions. We acknowledge support by the Austrian Science Fund FWF through the projects SFB FoQuS P13 and I1697-N27.

* Corresponding author: farokh.mivehvar@uibk.ac.at

† Corresponding author: helmut.ritsch@uibk.ac.at

- [1] M. Boninsegni and N. V. Prokof'ev, *Rev. Mod. Phys.* **84**, 759 (2012).
 [2] E. P. Gross, *Phys. Rev.* **106**, 161 (1957).
 [3] D. Thouless, *Ann. Phys. (N. Y.)* **52**, 403 (1969).
 [4] A. F. Andreev and I. M. Lifshitz, *Sov. Phys. JETP* **29**, 1107 (1969).

- [5] G. V. Chester, *Phys. Rev. A* **2**, 256 (1970).
 [6] A. J. Leggett, *Phys. Rev. Lett.* **25**, 1543 (1970).
 [7] E. Kim and M. H. W. Chan, *Nature* **427**, 225 (2004).
 [8] E. Kim and M. H. W. Chan, *Science* **305**, 1941 (2004).
 [9] J. Day and J. Beamish, *Nature* **450**, 853 (2007).
 [10] D. Y. Kim and M. H. W. Chan, *Phys. Rev. Lett.* **109**, 155301 (2012).
 [11] H. J. Maris, *Phys. Rev. B* **86**, 020502 (2012).
 [12] J.-R. Li, J. Lee, W. Huang, S. Burchesky, B. Shteynas, F. Ç. Top, A. O. Jamison, and W. Ketterle, *Nature* **543**, 91 (2017).
 [13] J. Léonard, A. Morales, P. Zupancic, T. Esslinger, and T. Donner, *Nature* **543**, 87 (2017).
 [14] I. Dimitrova, W. Lunden, J. Amato-Grill, N. Jepsen, Y. Yu, M. Messer, T. Rigaldo, G. Puentes, D. Weld, and W. Ketterle, *Phys. Rev. A* **96**, 051603 (2017).
 [15] S. Ostermann, F. Piazza, and H. Ritsch, *Phys. Rev. X* **6**, 021026 (2016).
 [16] S. Ostermann, F. Piazza, and H. Ritsch, *New J. Phys.* **19**, 125002 (2017).
 [17] D. Kruse, M. Ruder, J. Benhelm, C. von Cube, C. Zimmermann, P. W. Courteille, T. Elsässer, B. Nagorny, and A. Hemmerich, *Phys. Rev. A* **67**, 051802 (2003).
 [18] B. Nagorny, T. Elsässer, H. Richter, A. Hemmerich, D. Kruse, C. Zimmermann, and P. Courteille, *Phys. Rev. A* **67**, 031401 (2003).
 [19] S. Slama, G. Krenz, S. Bux, C. Zimmermann, and P. W. Courteille, *Phys. Rev. A* **75**, 063620 (2007).
 [20] S. Bux, H. Tomczyk, D. Schmidt, P. W. Courteille, N. Piovella, and C. Zimmermann, *Phys. Rev. A* **87**, 023607 (2013).
 [21] D. Schmidt, H. Tomczyk, S. Slama, and C. Zimmermann, *Phys. Rev. Lett.* **112**, 115302 (2014).
 [22] D. S. Naik, G. Kuyumjian, D. Pandey, P. Bouyer, and A. Bertoldi, *pre-print: arXiv:1712.06491* (2017).
 [23] M. G. Moore, O. Zobay, and P. Meystre, *Phys. Rev. A* **60**, 1491 (1999).
 [24] P. Horak and H. Ritsch, *Phys. Rev. A* **63**, 023603 (2001).
 [25] D. Nagy, J. K. Asbóth, P. Domokos, and H. Ritsch, *Europhysics Letters (EPL)* **74**, 254 (2006).
 [26] W. Chen, D. S. Goldbaum, M. Bhattacharya, and P. Meystre, *Phys. Rev. A* **81**, 053833 (2010).
 [27] S. Ostermann, T. Grieser, and H. Ritsch, *EPL (Europhysics Letters)* **109**, 43001 (2015).
 [28] H. Ritsch, P. Domokos, F. Brennecke, and T. Esslinger, *Rev. Mod. Phys.* **85**, 553 (2013).
 [29] K. Baumann, C. Guerlin, F. Brennecke, and T. Esslinger, *Nature* **464**, 1301 (2010).
 [30] J. Lang, F. Piazza, and W. Zwerger, *New J. Phys.* **19**, 123027 (2017).
 [31] R. I. Moodie, K. E. Ballantine, and J. Keeling, *pre-print: rXiv:1711.03915* (2017).
 [32] A. Morales, P. Zupancic, J. Lonard, T. Esslinger, and T. Donner, *pre-print: arXiv:1711.07988* (2017).
 [33] T. Grieser and H. Ritsch, *Phys. Rev. Lett.* **111**, 055702 (2013).
 [34] D. E. Chang, J. I. Cirac, and H. J. Kimble, *Phys. Rev. Lett.* **110**, 113606 (2013).
 [35] C. Maschler, H. Ritsch, A. Vukics, and P. Domokos, *Optics Communications* **273**, 446 (2007).
 [36] A. Vukics, C. Maschler, and H. Ritsch, *New J. Phys.* **9**, 255 (2007).
 [37] S. Krämer and H. Ritsch, *Phys. Rev. A* **90**, 033833 (2014).

- [38] J. Léonard, A. Morales, P. Zupancic, T. Donner, and T. Esslinger, *Science* **358**, 1415 (2017).
- [39] F. Piazza, P. Strack, and W. Zwerger, *Annals of Physics* **339**, 135 (2013).
- [40] See Supplemental Material for the details of the derivation of the mean-field equations, the linearized equations, and the threshold pump strength.
- [41] D. Nagy, G. Szirmai, and P. Domokos, *Eur. Phys. J. D* **48**, 127 (2008).
- [42] F. Mivehvar, F. Piazza, and H. Ritsch, *Phys. Rev. Lett.* **119**, 063602 (2017).
- [43] K. Baumann, R. Mottl, F. Brennecke, and T. Esslinger, *Phys. Rev. Lett.* **107**, 140402 (2011).
- [44] J. Jin, D. Rossini, R. Fazio, M. Leib, and M. J. Hartmann, *Phys. Rev. Lett.* **110**, 163605 (2013).
- [45] B. Bujnowski, J. K. Corso, A. L. C. Hayward, J. H. Cole, and A. M. Martin, *Phys. Rev. A* **90**, 043801 (2014).
- [46] R. Landig, L. Hruby, N. Dogra, M. Landini, R. Mottl, T. Donner, and T. Esslinger, *Nature* **532**, 476 (2016).
- [47] P. R. Berman, *Atom interferometry* (Academic press, 1997).
- [48] A. D. Cronin, J. Schmiedmayer, and D. E. Pritchard, *Rev. Mod. Phys.* **81**, 1051 (2009).
- [49] F. Sorrentino, K. Bongs, P. Bouyer, L. Cacciapuoti, M. de Angelis, H. Dittus, W. Ertmer, A. Giorgini, J. Hartwig, M. Hauth, S. Herrmann, M. Inguscio, E. Kajari, T. Knemann, C. Lmmerzahn, A. Landragin, G. Modugno, F. Pereira dos Santos, A. Peters, M. Prevedelli, E. Rasel, W. Schleich, M. Schmidt, A. Senger, K. Sengstock, G. Stern, G. Tino, and R. Walser, *Microgravity Science and Technology* **22**, 551 (2010).
- [50] P. Hamilton, M. Jaffe, J. M. Brown, L. Maisenbacher, B. Estey, and H. Müller, *Phys. Rev. Lett.* **114**, 100405 (2015).

SUPPLEMENTAL MATERIAL

Here we present the details of the derivation of the mean-field equations [Eq. (2) in the main text], the linearized equations [Eqs. (3) and (4) in the main text], and the threshold pump strength [Eq. (5) in the main text].

MEAN-FIELD EQUATIONS

The Heisenberg equations of motion of the photonic and atomic field operators can be obtained using the many-body effective Hamiltonian H_{eff} , given in the manuscript, as

$$\begin{aligned} i\hbar \frac{\partial}{\partial t} \hat{a}_{\pm} &= [\hat{a}_{\pm}, H_{\text{eff}}] = \hbar \left(-\Delta_c + U\hat{N} - i\kappa \right) \hat{a}_{\pm} + \hbar U \hat{N}_{\pm 2} \hat{a}_{\mp} + \hbar \eta \hat{N}_{\pm 1}, \\ i\hbar \frac{\partial}{\partial t} \hat{\psi} &= [\hat{\psi}, H_{\text{eff}}] = \mathcal{H}_{\text{eff}}^{(1)} \hat{\psi}, \end{aligned} \quad (\text{S1})$$

where $\hat{N} = \int \hat{\psi}^\dagger(x) \hat{\psi}(x) dx$, $\hat{N}_{\pm 1} \equiv \int \hat{\psi}^\dagger(x) e^{\mp i k_c x} \hat{\psi}(x) dx$, and $\hat{N}_{\pm 2} \equiv \int \hat{\psi}^\dagger(x) e^{\mp 2i k_c x} \hat{\psi}(x) dx$. Here we have added field damping terms proportional to the cavity decay rate κ . By replace the photonic and atomic field operators with their corresponding quantum averages, $\hat{a}_{\pm}(t) \rightarrow \langle \hat{a}_{\pm}(t) \rangle = \alpha_{\pm}(t) = |\alpha_{\pm}(t)| e^{i\phi_{\pm}(t)}$ and $\hat{\psi}(x, t) \rightarrow \langle \hat{\psi}(x, t) \rangle = \psi(x, t) = \sqrt{n(x, t)} e^{i\theta(t)}$, respectively, one obtains the three mean-field coupled equations (2) in the manuscript.

LINEARIZED EQUATIONS

Assuming $\psi(x, t) = e^{-i\mu_0 t/\hbar} [\psi_0(x) + \delta\psi(x, t)]$ and $\alpha_{\pm}(t) = \alpha_{0\pm} + \delta\alpha_{\pm}(t)$, where $\psi_0(x)$ and $\alpha_{0\pm}$ are the mean-field stationary-state solutions of Eq. (2) in the main text with the chemical potential μ_0 , linearizing Eq. (2) yields

$$\begin{aligned} i \frac{\partial}{\partial t} \delta\alpha_{\pm} &= (-\Delta_c + UN - i\kappa) \delta\alpha_{\pm} + U \mathcal{N}_{\pm 2}^{(0)} \delta\alpha_{\mp} + \int A_{\pm} (\psi_0^* \delta\psi + \psi_0 \delta\psi^*) dx, \\ i \frac{\partial}{\partial t} \delta\psi &= \frac{1}{\hbar} \left(\mathcal{H}_{\text{eff}}^{(1)} - \mu_0 \right) \delta\psi + \psi_0 \left(A_+^* \delta\alpha_+ + A_+ \delta\alpha_+^* + A_-^* \delta\alpha_- + A_- \delta\alpha_-^* \right), \end{aligned} \quad (\text{S2})$$

where $\mathcal{N}_{\pm 2}^{(0)} = \int n_0(x) e^{\mp 2i k_c x} dx$ and we have defined $A_{\pm}(x) \equiv U (\alpha_{0\pm} + \alpha_{0\mp} e^{\mp 2i k_c x}) + \eta e^{\mp i k_c x}$ for shorthands. Since the linearized equations (S2) couple $\delta\psi$ and $\delta\alpha_{\pm}$ to their complex conjugates, we make the ansätze $\delta\psi(x, t) = \delta\psi^{(+)}(x) e^{-i\omega t} + [\delta\psi^{(-)}(x)]^* e^{i\omega^* t}$ and $\delta\alpha_{\pm}(t) = \delta\alpha_{\pm}^{(+)} e^{-i\omega t} + [\delta\alpha_{\pm}^{(-)}]^* e^{i\omega^* t}$ for the quantum fluctuations. Substituting these ansätze in Eq. (S2) and setting the coefficients of $e^{-i\omega t}$ and $e^{i\omega^* t}$ separately to zero yields a set of six coupled Bogoliubov-type equations for the positive- and negative-frequency components of the quantum fluctuations,

$$\omega \delta\alpha_{\pm}^{(+)} = (-\Delta_c + UN - i\kappa) \delta\alpha_{\pm}^{(+)} + U \mathcal{N}_{\pm 2}^{(0)} \delta\alpha_{\mp}^{(+)} + \int A_{\pm} \left[\psi_0^* \delta\psi^{(+)} + \psi_0 \delta\psi^{(-)} \right] dx,$$

$$\begin{aligned}
\omega \delta \alpha_{\pm}^{(-)} &= -(-\Delta_c + UN - i\kappa)^* \delta \alpha_{\pm}^{(-)} - UN_{\pm 2}^{(0)*} \delta \alpha_{\mp}^{(-)} - \int A_{\pm}^* \left[\psi_0^* \delta \psi^{(+)} + \psi_0 \delta \psi^{(-)} \right] dx, \\
\omega \delta \psi^{(+)} &= \frac{1}{\hbar} \left[\mathcal{H}_{\text{eff}}^{(1)} - \mu_0 \right] \delta \psi^{(+)} + \psi_0 \left[A_+^* \delta \alpha_+^{(+)} + A_+ \delta \alpha_+^{(-)} + A_-^* \delta \alpha_-^{(+)} + A_- \delta \alpha_-^{(-)} \right], \\
\omega \delta \psi^{(-)} &= -\frac{1}{\hbar} \left[\mathcal{H}_{\text{eff}}^{(1)} - \mu_0 \right] \delta \psi^{(-)} - \psi_0^* \left[A_+^* \delta \alpha_+^{(+)} + A_+ \delta \alpha_+^{(-)} + A_-^* \delta \alpha_-^{(+)} + A_- \delta \alpha_-^{(-)} \right].
\end{aligned} \tag{S3}$$

We recast these equations in a matrix form

$$\omega \mathbf{f} = \mathbf{M}_B \mathbf{f}, \tag{S4}$$

where $\mathbf{f} = (\delta \alpha_+^{(+)}, \delta \alpha_+^{(-)}, \delta \alpha_-^{(+)}, \delta \alpha_-^{(-)}, \delta \psi^{(+)}, \delta \psi^{(-)})^T$ and

$$\mathbf{M}_B = \begin{pmatrix} \delta_c & 0 & UN_{+2}^{(0)} & 0 & \mathcal{I}_{+*} & \mathcal{I}_{+} \\ 0 & -\delta_c^* & 0 & -UN_{+2}^{(0)*} & -\mathcal{I}_{+}^* & -\mathcal{I}_{+*}^* \\ UN_{-2}^{(0)} & 0 & \delta_c & 0 & \mathcal{I}_{-*} & \mathcal{I}_{-} \\ 0 & -UN_{-2}^{(0)*} & 0 & -\delta_c^* & -\mathcal{I}_{-}^* & -\mathcal{I}_{-*}^* \\ \psi_0 A_+^* & \psi_0 A_+ & \psi_0 A_-^* & \psi_0 A_- & (\mathcal{H}_{\text{eff}}^{(1)} - \mu_0)/\hbar & 0 \\ -\psi_0^* A_+^* & -\psi_0^* A_+ & -\psi_0^* A_-^* & -\psi_0^* A_- & 0 & -(\mathcal{H}_{\text{eff}}^{(1)} - \mu_0)/\hbar \end{pmatrix}, \tag{S5}$$

with $\delta_c \equiv -\Delta_c + UN - i\kappa$. Here we have introduced the integral operators,

$$\begin{aligned}
\mathcal{I}_{\pm} \xi &= \int A_{\pm}(x) \psi_0(x) \xi dx, \\
\mathcal{I}_{\pm*} \xi &= \int A_{\pm}(x) \psi_0^*(x) \xi dx.
\end{aligned} \tag{S6}$$

We find eigenvalues ω of Eq. (S4) by numerically diagonalizing the Bogoliubov matrix (S5) on one unit cell (of length λ_c) with a periodic boundary condition. We discretize the space and replace the kinetic energy term $-(\hbar^2/2m)\partial_x^2$ and the integral operators $\{\mathcal{I}_{\pm}, \mathcal{I}_{\pm*}\}$ with the corresponding finite-difference terms.

The Threshold Pump Strength

In order to find an analytical equation for the critical threshold, we analyze the stability of the the trivial solution (i.e., the solution below the Dicke transition) $\alpha_{0\pm} = 0$ and $\psi_0 = \sqrt{N/\lambda_c}$ with $\mu_0 = 0$, by restricting the atomic fluctuations to the momentum states $\pm \hbar k_c$. Using this trivial solution and the ansatz $\delta \psi^{(\pm)}(x) = \delta \psi_{\pm}^{(\pm)} e^{ik_c x} + \delta \psi_{\mp}^{(\pm)} e^{-ik_c x}$ for the positive- and negative-frequency condensate fluctuations with momenta $\pm \hbar k_c$, the Bogoliubov matrix (S5) takes the following form,

$$\tilde{\mathbf{M}}_B = \begin{pmatrix} \delta_c & 0 & 0 & 0 & \sqrt{N\lambda_c}\eta & \sqrt{N\lambda_c}\eta & 0 & 0 \\ 0 & -\delta_c^* & 0 & 0 & 0 & 0 & -\sqrt{N\lambda_c}\eta & -\sqrt{N\lambda_c}\eta \\ 0 & 0 & \delta_c & 0 & 0 & 0 & \sqrt{N\lambda_c}\eta & \sqrt{N\lambda_c}\eta \\ 0 & 0 & 0 & -\delta_c^* & -\sqrt{N\lambda_c}\eta & -\sqrt{N\lambda_c}\eta & 0 & 0 \\ \sqrt{N/\lambda_c}\eta & 0 & 0 & \sqrt{N/\lambda_c}\eta & \omega_r & 0 & 0 & 0 \\ -\sqrt{N/\lambda_c}\eta & 0 & 0 & -\sqrt{N/\lambda_c}\eta & 0 & -\omega_r & 0 & 0 \\ 0 & \sqrt{N/\lambda_c}\eta & \sqrt{N/\lambda_c}\eta & 0 & 0 & 0 & \omega_r & 0 \\ 0 & -\sqrt{N/\lambda_c}\eta & -\sqrt{N/\lambda_c}\eta & 0 & 0 & 0 & 0 & -\omega_r \end{pmatrix}. \tag{S7}$$

The eigenvalues ω of $\tilde{\mathbf{M}}_B$ is obtained via the eighth-order characteristic equation $\text{Det}(\tilde{\mathbf{M}}_B - \omega I_{8 \times 8}) = 0$:

$$[(\omega^2 - \omega_r^2)(\omega - \delta_c)(\omega + \delta_c^*) + 4N\eta^2\omega_r(\Delta_c - UN)]^2 = 0. \tag{S8}$$

The solution of the characteristic equation (S8) yields the spectra ω of the atomic and photonic excitations, which below the threshold η_c are in excellent agreement with the first and last excitation bands of Fig. 3 in the manuscript obtained from the full numerical calculations. Above η_c the solutions of Eq. (S8) develop positive imaginary parts,

signaling that the trivial solution $\alpha_{0\pm} = 0$ and $\psi_0 = \sqrt{N/\lambda_c}$ is unstable towards the superradiant phase. The zero-frequency solution $\omega = 0$ of the characteristic equation (S8) yields the self-ordering threshold,

$$\sqrt{N}\eta_c = \sqrt{\frac{(-\Delta_c + UN)^2 + \kappa^2}{4(-\Delta_c + UN)}}\sqrt{\omega_r}. \quad (\text{S9})$$